Small two-component Fermi gases in a cubic box with periodic boundary conditions

X. Y. Yin[1] and D. Blume[1, 2]

[1] *Department of Physics and Astronomy, Washington State University, Pullman, Washington 99164 USA*
[2] *ITAMP, Harvard-Smithsonian Center for Astrophysics, Cambridge, Massachusetts 02138, USA*

(Dated: June 18, 2018)

The properties of two-component Fermi gases become universal if the interspecies s-wave scattering length a_s and the average interparticle spacing are much larger than the range of the underlying two-body potential. Using an explicitly correlated Gaussian basis set expansion approach, we determine the eigen energies of two-component Fermi gases in a cubic box with periodic boundary conditions as functions of the interspecies s-wave scattering length and the effective range of the two-body potential. The universal properties of systems consisting of up to four particles are determined by extrapolating the finite-range energies to the zero-range limit. We determine the eigen energies of states with vanishing and finite momentum. In the weakly-attractive BCS regime, we analyze the energy spectra and degeneracies using first-order degenerate perturbation theory. Excellent agreement between the perturbative energy shifts and the numerically determined energies is obtained. For the infinitely large scattering length case, we compare our results—where available—with those presented in the literature.

PACS numbers:

I. INTRODUCTION

Two-component Fermi gases with interspecies contact interactions have emerged as a paradigm of strongly-correlated systems [1–5]. A detailed understanding of the equation of state of two-component Fermi gases as functions of the strength of the contact interaction and the temperature is, e.g., of importance to nuclear and astrophysics. Dilute ultracold atomic ^{6}Li and ^{40}K gases provide nearly ideal table-top realizations of this paradigm system. Indeed, much of our current understanding of strongly-correlated Fermi systems throughout the BCS-BEC crossover and at unitarity comes from a host of experimental cold atom studies. These experimental studies are complemented by theoretical studies.

When the s-wave scattering length, which can be tuned through the application of an external magnetic field in the vicinity of a Fano-Feshbach resonance [6], becomes large, the system does not possess a small parameter and non-perturbative approaches are needed. In this regime, the equation of state of two-component Fermi gases has been determined by Monte Carlo as well as other non-perturbative methods [1, 7–13]. While the fixed-node diffusion Monte Carlo method yields variational upper bounds, other Monte Carlo methods are expected to provide, within the statistical uncertainty, essentially exact results [7–10, 12]. In assessing the accuracy of the various theoretical approaches, exact diagonalization schemes of small model systems play a crucial role [14]. The explicitly correlated Gaussian basis set expansion approach has been used extensively to treat two-component Fermi gases under harmonic confinement [15–21]. The present work extends the standard explicitly correlated Gaussian approach [22, 23] to study few-body systems in a cubic box with periodic boundary conditions. The method introduced in this paper is directly applicable to other periodic systems such as atoms loaded into optical lattices. In addition to serving as a benchmark, our study of strongly-correlated few-body systems in a cubic box with periodic boundary conditions aids in developing a physical understanding of the corresponding many-body systems. The results are also relevant to the analysis of on-going lattice QCD simulations [24–26].

This work considers equal-mass Fermi gases consisting of N_1 spin-up fermions and N_2 spin-down fermions in a cubic box of length L with periodic boundary conditions. We consider the regime where the unlike particles do not interact and where the interspecies interactions are characterized by a short-range potential with s-wave scattering length a_s and effective range r_{eff}. The key points of this paper are: *(i)* We introduce explicitly correlated Gaussian basis functions and show that the resulting basis, constructed using the stochastic variational approach [27], provides an accurate description of few-body states with vanishing and non-vanishing momentum. Compact analytic expressions for the most important matrix elements are reported. *(ii)* We analyze the energy spectra and degeneracies of the $(N_1, N_2) = (1,1)$, $(2,1)$, $(2,2)$ and $(3,1)$ systems in the weakly-attractive BCS regime (i.e., for $|a_s|/L \ll 1$ and $a_s < 0$) using first-order degenerate perturbation theory. *(iii)* Tables II-IV present accurate results for the ground state energies of the $(N_1, N_2) = (1,1)$, $(2,1)$, $(2,2)$ and $(3,1)$ systems, and the excited states of the $(1,1)$ and $(2,1)$ systems at unitarity. Our extrapolated zero-range energy of the $(2,2)$ system is in excellent agreement with earlier benchmark results [14]. *(iv)* We present energy spectra throughout the BEC-BCS crossover.

The remainder of this paper is organized as follows. Section II discusses the theoretical framework. Specifically, Sec. II A introduces the system Hamiltonian, Sec. II B discusses the degenerate perturbation theory treatment of the weakly-attractive BCS regime, and Sec. II C introduces the explicitly correlated Gaussian basis set expansion approach. Section III presents our results for the $(1,1)$, $(2,1)$, $(2,2)$ and $(3,1)$ systems. Lastly, Sec. IV concludes. Details of the explicitly correlated Gaussian basis functions for systems with periodic boundary conditions are relegated to the Appendix.

II. THEORETICAL FRAMEWORK

A. System Hamiltonian

We study equal-mass two-component Fermi gases consisting of N_1 spin-up and N_2 spin-down atoms ($N = N_1 + N_2$) in a cubic box of length L with periodic boundary conditions. Besides the box, the particles feel no external forces. The system Hamiltonian H reads

$$H = H_0 + V_{\text{int}}, \tag{1}$$

where H_0,

$$H_0 = \sum_{a=1}^{N} -\frac{\hbar^2}{2m}\nabla_a^2, \tag{2}$$

is the non-interacting Hamiltonian and V_{int},

$$V_{\text{int}} = \sum_{a=1}^{N_1} \sum_{b=N_1+1}^{N} V_{\text{tb}}(\mathbf{x}_{ab}), \tag{3}$$

is the pairwise additive interaction potential. In Eq. (2), m denotes the atom mass and ∇_a^2 the Laplacian of the ath atom with position vector $\mathbf{x}_a$. The two-body interaction potential V_{tb} depends on the interparticle distance vector $\mathbf{x}_{ab}$, where $\mathbf{x}_{ab} = \mathbf{x}_a - \mathbf{x}_b$.

We consider two different short-range model potentials $V_{\text{tb}}(\mathbf{x}_{ab})$. Our perturbative treatment (see Sec. II B) employs the bare or non-regularized Fermi pseudopotential V_{F} [28],

$$V_{\text{F}}(\mathbf{x}_{ab}) = \frac{4\pi\hbar^2 a_s}{m}\delta^{(3)}(\mathbf{x}_{ab}), \tag{4}$$

where a_s is the two-body free-space s-wave scattering length. Our explicitly correlated Gaussian basis set expansion approach (see Secs. II C and III), in contrast, employs a finite-range Gaussian potential V_{g} with range r_0 and depth U_0,

$$V_{\text{g}}(\mathbf{x}_{ab}) = U_0 \exp\left(-\frac{\mathbf{x}_{ab}^2}{2r_0^2}\right). \tag{5}$$

For a fixed r_0, U_0 ($U_0 < 0$) is adjusted to generate potentials with different a_s. Throughout, we restrict ourselves to two-body potentials that support zero and one two-body s-wave bound states in free space for a_s negative and positive, respectively.

B. Perturbative treatment

In the weakly-attractive regime, i.e., for $|a_s|/L \ll 1$ ($a_s < 0$), we treat the two-component Fermi gas in a cubic box with periodic boundary conditions perturbatively. Specifically, the potential V_{int} with $V_{\text{tb}} = V_{\text{F}}$, see Eqs. (3) and (4), is treated as a perturbation to the non-interacting Hamiltonian H_0, Eq. (2). Using standard first-order degenerate time-independent perturbation theory, we determine the leading-order energy shifts of the non-interacting energy levels and corresponding degeneracies. Moreover, we construct properly anti-symmetrized eigen states that simultaneously diagonalize H_0 and the total momentum operator.

The unsymmetrized eigen states $\Phi^{(0)}$ of the unperturbed Hamiltonian H_0, Eq. (2), with periodic boundary conditions are most conveniently written in terms of plane wave states,

$$\Phi^{(0)}_{\mathbf{k}_1,\cdots,\mathbf{k}_N}(\mathbf{x}_1,\cdots,\mathbf{x}_N) = \frac{1}{L^{3N/2}}\prod_{a=1}^{N}\exp(\imath\mathbf{k}_a\cdot\mathbf{x}_a), \tag{6}$$

where the wave vectors $\mathbf{k}_a$ satisfy the condition

$$\mathbf{k}_a = \frac{2\pi}{L}\mathbf{n}_a \tag{7}$$

with $\mathbf{n}_a = (n_a^{(1)}, n_a^{(2)}, n_a^{(3)})$ and $n_a^{(j)} = 0, 1, \cdots$. The corresponding unperturbed eigen energies $E_n^{(0)}$ read

$$E_n^{(0)} = nE_{\text{box}}, \tag{8}$$

where

$$E_{\text{box}} = \frac{2\pi^2\hbar^2}{mL^2} \tag{9}$$

and

$$n = \sum_{a=1}^{N}\mathbf{n}_a^2. \tag{10}$$

As can be seen from Eqs. (8) and (10), the energies $E_n^{(0)}$ are, except for the lowest state with $n = 0$, degenerate.

We obtain the energy shifts $\Delta E_{n,q}$ of the energy level $E_n^{(0)}$ by diagonalizing the matrix

$$\langle\Phi^{(0)}_{\mathbf{k}_1,\cdots,\mathbf{k}_N}|V_{\text{int}}|\Phi^{(0)}_{\mathbf{k}'_1,\cdots,\mathbf{k}'_N}\rangle, \tag{11}$$

which is constructed using the unperturbed states $\Phi^{(0)}_{\mathbf{k}_1,\cdots,\mathbf{k}_N}$ and $\Phi^{(0)}_{\mathbf{k}'_1,\cdots,\mathbf{k}'_N}$ with energy $E_n^{(0)}$. As a result of the interaction, each degenerate non-interacting energy $E_n^{(0)}$ is split into Q sublevels with distinct energy shift $\Delta E_{n,q}$ ($q = 1, \cdots, Q$) and $|\mathbf{K}|$ (see below). The non-interacting states that diagonalize the perturbation matrix, Eq. (11), are also eigenstates of the total momentum operator $\mathbf{P}$,

$$\mathbf{P} = -\imath\hbar\sum_{a=1}^{N}\nabla_a, \tag{12}$$

TABLE I: Perturbative treatment of $(1,1)$, $(2,1)$, $(2,2)$ and $(3,1)$ systems. Column two shows the non-interacting energy $E_n^{(0)}$. Columns three and four report the first-order energy shift $\Delta E_{n,q}$ and the magnitude of the total wave vector $|\mathbf{K}|$. The degeneracy of each state is shown in column five.

(N_1, N_2)	$E_n^{(0)}/E_{\text{box}}$	$\Delta E_{n,q}/(\frac{4\pi\hbar^2 a_s}{mL^3})$	$\lvert\mathbf{K}\rvert/(\frac{2\pi}{L})$	Deg.
(1, 1)	0	1	0	1
	1	2	1	6
		0	1	6
	2	6	0	1
		4	$\sqrt{2}$	12
		1	2	6
		0	0	5
		0	$\sqrt{2}$	36
(2, 1)	1	2	1	6
	2	7	0	1
		4	$\sqrt{2}$	12
		3	0	3
		3	$\sqrt{2}$	12
		2	2	6
		1	0	2
		1	$\sqrt{2}$	12
		0	0	3
		0	$\sqrt{2}$	12
(2, 2)	2	9	0	1
		5	$\sqrt{2}$	12
		4	2	6
		3	0	5
		3	$\sqrt{2}$	12
(3, 1)	2	3	0	3
		3	$\sqrt{2}$	12

with eigenvalue $\hbar\mathbf{K}$, where $\mathbf{K} = \sum_{a=1}^{N} \mathbf{k}_a$.

Up to this point, no symmetry constraints have been imposed. To construct states with proper fermionic exchange symmetry, we form all possible linear combinations of states that satisfy the anti-symmetry requirement under the interchange of pairs of identical fermions for each manifold labeled by $\Delta E_{n,q}$ and $\hbar|\mathbf{K}|$.

Table I summarizes the energy shifts $\Delta E_{n,q}$, the magnitude of the total momentum $\hbar|\mathbf{K}|$, and the corresponding degeneracies for the lowest few states of the $(1,1)$, $(2,1)$, $(2,2)$ and $(3,1)$ Fermi systems. For the $(1,1)$ system, the lowest non-interacting state is one-fold degenerate and is characterized by a perturbation shift of $\Delta E_{n,q} = 4\pi\hbar^2 a_s/(mL^3)$ and magnitude of total momentum of $\hbar|\mathbf{K}| = 0$. The first excited and second excited non-interacting states, in contrast, are 12-fold and 60-fold degenerate, respectively. The degeneracy of 12 arises since plane wave states with $\mathbf{K}/(2\pi/L) = (\pm1,0,0)$, $(0,\pm1,0)$ and $(0,0,\pm1)$ are degenerate. Moreover, the state with $\mathbf{K}/(2\pi/L) = (1,0,0)$, e.g., can be constructed by putting either the first or the second particle into the first excited state, yielding a total degeneracy of 12. The interactions split the first excited state into two levels with degeneracy six each. One level is shifted down by the attractive interactions, while the other is unshifted, reflecting the fact that the wave function vanishes when the two particles sit on top of each other. The second excited state, which has a degeneracy of 60 in the absence of interactions, is split into five levels with distinct $\Delta E_{n,q}$ and $|\mathbf{K}|$ "labels".

For $N = 3$ and 4, the counting of the degeneracies is more involved than for the $(1,1)$ system, since the (unperturbed) non-interacting wave functions have to be anti-symmetric under the exchange of identical fermions. The fact that the non-interacting ground state of the $(2,1)$, $(2,2)$ and $(3,1)$ systems has a finite energy, and not a vanishing energy as in the $(1,1)$ case, is a direct consequence of the fermionic anti-symmetry requirement. Another interesting aspect of the results summarized in Table I is that the ground state of the $(2,1)$ system has, in the weakly-attractive regime, a finite momentum while the ground state of the $(2,2)$ system has a vanishing momentum. Interestingly, the first-order perturbation theory shift of the lowest two levels of the $(3,1)$ system, which have vanishing and finite momentum, respectively, is identical. The momentum of the true ground state in the BCS regime can thus not be determined within first-order perturbation theory but requires the determination of higher-order corrections or the usage of a non-perturbative technique.

The perturbative treatment breaks down when $|a_s|/L$ is not small compared to 1. To treat systems with arbitrary s-wave scattering length a_s, we resort to a numerical approach, the explicitly correlated Gaussian approach.

C. Explicitly correlated Gaussian basis set expansion approach

To numerically solve the time-independent Schrödinger equation for the Hamiltonian given in Eq. (1), we employ the finite-range two-body model potential defined in Eq. (5). We expand the wave function in terms of explicitly correlated Gaussian basis functions [22, 23], which depend on a set of non-linear variational parameters. These non-linear parameters are optimized semi-stochastically [27] by minimizing the energy of the state of interest. Since the basis functions are not linearly independent, the eigen energies are obtained by solving a generalized eigen value problem that involves the Hamiltonian matrix and the overlap matrix [22, 23].

In the cold atom context, explicitly correlated Gaussian basis sets have been applied extensively to harmonically trapped few-body systems [15–21]. However, this approach has not yet been extended to cold atom systems with periodic boundary conditions [29]. To treat periodic systems, we imagine that the full three-dimensional space is divided into an infinite number of cubic boxes of length L. We place the N particles in the "center box". The center box defines our system of interest. We then imagine that the particles in the center box are copied to all other boxes, i.e., we shift all position vectors $\mathbf{x}_a$ $(a = 1, \cdots, N)$ by $(Lb_a^{(1)}, Lb_a^{(2)}, Lb_a^{(3)})$, where the $b_a^{(j)}$ take the values $\cdots, -2, -1, 0, 1, \cdots$. Correspondingly, we enforce the periodicity of the basis functions by explicitly summing over all possible $b_a^{(j)}$. The explicit functional form of the basis functions as well as compact expressions for the Hamiltonian matrix element and the overlap matrix element are given in the Appendix.

In practice, we can only treat a finite and not an infinite number of boxes. Our calculations reported in Sec. III employ 9^3 boxes for the $(1,1)$ and $(2,1)$ systems, and 7^3 boxes for the $(2,2)$ and $(3,1)$ systems. We estimate that the error caused by using a finite and not an infinite number of boxes is of the order of 0.0001% for the $(1,1)$ and $(2,1)$ systems and of the order of 0.001% for the $(2,2)$ and $(3,1)$ systems, respectively. For the $(2,1)$, $(2,2)$ and $(3,1)$ systems, this error is significantly smaller than the basis set extrapolation error and the error arising from extrapolating the finite-range energies to the zero-range limit (see Sec. III for details).

One of the challenges in constructing numerically tractable basis sets applicable to cold atom systems is that the system dynamics depends on the range r_0 of the underlying two-body potential as well as the box length L, where $r_0 \ll L$. As we will demonstrate in Sec. III, our basis functions are flexible enough to describe short-range correlations that occur at the length scale of r_0 and long-range correlations that occur at the length scale of L. Our scheme to optimize the non-linear parameters roughly follows that discussed in Refs. [21, 22]. In particular, we construct separate basis sets for each state of interest. When optimizing highly excited states, we first perform a rough minimization of the energy of all lower-lying states and then use the majority of the basis functions to minimize the energy of the state of interest. The calculations reported in Sec. III use of the order of $N_b = 500$, where N_b is the number of unsymmetrized basis functions.

III. RESULTS

This section discusses the energies of the $(1,1)$, $(2,1)$, $(2,2)$ and $(3,1)$ systems obtained by the explicitly correlated Gaussian basis set expansion approach. Throughout, we refer to these energies as ECG energies.

Figure 1(a) shows the energies of the four lowest states of the $(1,1)$ system at unitarity as a function of the effective range r_{eff}. The effective range is defined through the low-energy expansion of the two-body free-space s-wave scattering length [30]. The lowest state shown in Fig. 1(a) is one-fold degenerate and has vanishing momentum $\hbar\mathbf{K}$. The second state has $\hbar|\mathbf{K}| = 2\pi\hbar/L$ and is six-fold degenerate. The third and fourth states cross at $r_{\text{eff}}/L \approx 0.04$. The state that is essentially unaffected by the interactions [dash-dotted line in Fig. 1(a)] is six-fold degenerate; in the weakly-attractive regime, this state is characterized by $\Delta E_{n,q} = 0$. The state that is more strongly affected by the interactions [dash-dot-dotted line in Fig. 1(a)] is one-fold degenerate and has vanishing momentum $\hbar\mathbf{K}$.

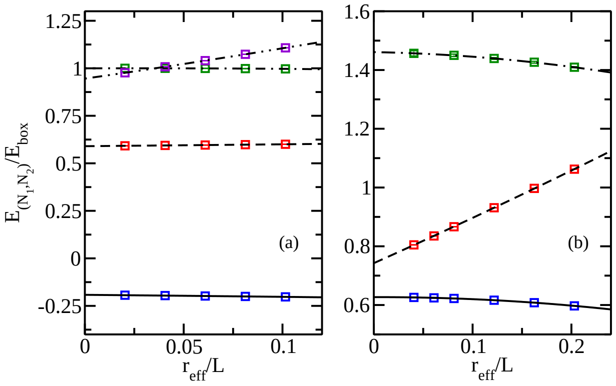

FIG. 1: (Color online) (a) The four lowest $(1,1)$ states and (b) the three lowest $(2,1)$ states at unitarity as a function of the effective range r_{eff}. For the Gaussian potential V_{g}, we find $r_{\text{eff}} \approx 2.03 r_0$. Squares with error bars show the ECG energies extrapolated to the $N_b \to \infty$ limit (the error bars are hardly visible on the scale shown). The lines show fits.

Table II lists the $(1,1)$ energies for different r_0. The fourth column reports the energies for the largest basis set considered; according to the variational principle [22, 23], these ECG energies provide upper bounds to the exact eigen energies. The third column reports the energies obtained by extrapolating the ECG energies to the infinite basis set limit. To extrapolate the finite-range energies to the zero-range limit, we perform separate three or four parameter fits to the energies listed in the third and fourth columns of Table II. The $N_b \to \infty$ energies, extrapolated to the zero-range limit, are our best estimates for the zero-range energies. The associated error bars (see Table II) are obtained by taking the difference between the extrapolated zero-range energies reported in columns three and four. Imposing the Bethe-Peierls boundary condition for zero-range interactions on the two-body wave function, the zero-range energies for states with $\mathbf{K} = 0$ can be found with very high accuracy [31, 32] (in nuclear physics, the resulting implicit eigen equation is known as "Lüscher formula"). For the two lowest $\mathbf{K} = 0$ levels one finds $E = -0.19180 E_{\text{box}}$ and $E = 0.94579 E_{\text{box}}$, respectively. Our zero-range energies [$E = -0.19182(2) E_{\text{box}}$ and $E = 0.94572(16) E_{\text{box}}$, see Table II] agree with the exact energies within error bars. Our energy of $E = 0.59019(50) E_{\text{box}}$ for the lowest state with $\hbar|\mathbf{K}| = 2\pi\hbar/L$ agrees with the value of $E = 0.5902 E_{\text{box}}$ obtained by Werner and Castin [33].

Figure 1(b) and Table III summarize our results for the $(2,1)$ system at unitarity. The lowest state of the $(2,1)$ system at unitarity is six-fold degenerate and has $\hbar|\mathbf{K}| = 2\pi\hbar/L$, while the second and third states are one-fold and three-fold degenerate, respectively, and have $\hbar|\mathbf{K}| = 0$. The $(2,1)$ energies at unitarity have previously been determined by a variety of methods, including a continuum Green's function approach [24] and lattice Monte Carlo techniques [13, 14]. While states with vanishing momentum have been considered frequently, we

TABLE II: Energies of the four lowest states of the $(1,1)$ system at unitarity for different r_0. The fourth column reports the lowest ECG energy for each r_0 (i.e., the energy for the largest basis set considered). The third column reports the energies extrapolated to the infinite basis set limit, i.e., for $N_b \to \infty$. The $r_0 = 0$ energies are obtained by extrapolating the finite-range energies to the zero-range limit. The error bar for the $r_0 = 0$ energy reported in the third column is obtained by taking the difference between the $r_0 = 0$ energies reported in columns three and four. Column five reports the magnitude of the wave vector $|\mathbf{K}|$.

state	r_0/L	E/E_{box} $N_b \to \infty$	E/E_{box} largest N_b	$\lvert\mathbf{K}\rvert/\left(\frac{2\pi}{L}\right)$
1	0.05	−0.20259	−0.20259	0
	0.04	−0.20025	−0.20025	
	0.03	−0.19801	−0.19801	
	0.02	−0.19586	−0.19585	
	0.01	−0.19379	−0.19378	
	0	−0.19182(2)	−0.19180	
2	0.05	0.60026	0.60030	1
	0.04	0.59816	0.59820	
	0.03	0.59610	0.59623	
	0.02	0.59410	0.59437	
	0.01	0.59211	0.59245	
	0	0.59019(50)	0.59069	
3	0.05	1.10766	1.10767	0
	0.04	1.07358	1.07359	
	0.03	1.04024	1.04026	
	0.02	1.00778	1.00784	
	0.01	0.97623	0.97634	
	0	0.94572(16)	0.94588	
4	0.05	0.99689	0.99692	1
	0.04	0.99840	0.99842	
	0.03	0.99931	0.99935	
	0.02	0.99979	0.99982	
	0.01	0.99997	1.00000	
	0	1.00000(2)	1.00002	

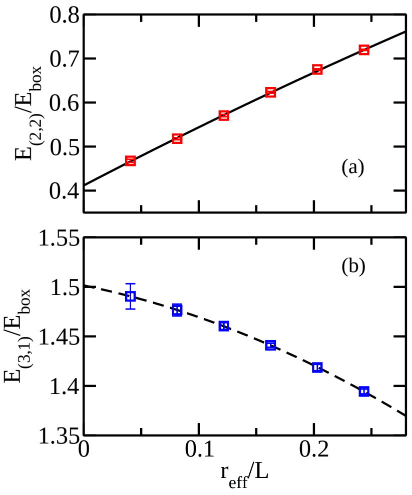

FIG. 2: (Color online) Energy of the lowest state of (a) the $(2,2)$ system and (b) the $(3,1)$ system at unitarity as a function of r_{eff}. See caption of Fig. 1 for details.

TABLE III: Energies of the three lowest levels of the $(2,1)$ system at unitarity for different r_0. See caption of Table II for details. For the first excited state, the difference between the zero-range energies E/E_{box} calculated for infinite and finite N_b is very small; we estimate that this difference underestimates the "true" error bar.

state	r_0/L	E/E_{box} $N_b \to \infty$	E/E_{box} largest N_b	$\lvert\mathbf{K}\rvert/\left(\frac{2\pi}{L}\right)$
1	0.1	0.5971	0.5973	1
	0.08	0.6080	0.6085	
	0.06	0.6164	0.6168	
	0.04	0.6223	0.6227	
	0.03	0.6244	0.6256	
	0.02	0.6259	0.6270	
	0.01	0.6274	0.6295	
	0	0.6282(30)	0.6312	
2	0.1	1.0625	1.0626	0
	0.08	0.9971	0.9972	
	0.06	0.9312	0.9314	
	0.04	0.8665	0.8668	
	0.03	0.8352	0.8356	
	0.02	0.8047	0.8051	
	0	0.7424(6)	0.7430	
3	0.1	1.4095	1.4112	0
	0.08	1.4256	1.4287	
	0.06	1.4392	1.4421	
	0.04	1.4500	1.4540	
	0.02	1.4567	1.4657	
	0	1.4609(132)	1.4741	

are aware of only one study that considered states with finite total momentum [34]. Our energies for the second and third states agree, within error bars, with the literature values [24]. Our estimate for the $(2,1)$ zero-range ground state energy at unitarity is $E = 0.6282(30)E_{\text{box}}$. The fact that the ground state has finite total momentum is a direct consequence of the anti-symmetry requirement of the wave function under the interchange of the two identical fermions. This is analogous to the harmonically trapped $(2,1)$ system at unitarity with zero-range interactions, which is characterized by a total orbital angular momentum of $L = 1$ [18, 35, 36].

Figure 2 and Table IV summarize our results for the lowest state of the $(2,2)$ and $(3,1)$ systems at unitarity. These states are one-fold and three-fold degenerate, respectively, and have $\hbar|\mathbf{K}| = 0$. The ground state energy of the $(2,2)$ system has been benchmarked previously [14]. Reference [14] finds $E = 0.422(4)E_{\text{box}}$ and $0.420(4)E_{\text{box}}$ using two different lattice representations of the Hamiltonian, $E = 0.412(18)E_{\text{box}}$ using a Euclidean lattice approach, and an upper bound of $E = 0.424(4)E_{\text{box}}$ using the fixed-node diffusion Monte Carlo approach. Our extrapolated zero-range energy of $E = 0.4116(42)E_{\text{box}}$ agrees with these results within error bars. Note that our error bar is comparable to those of Ref. [14]. For the $(3,1)$ system, we are not aware of any literature results.

Symbols in Figs. 3(a) and 3(b) show the lowest few

TABLE IV: Energies of the lowest state of the $(2,2)$ and $(3,1)$ systems at unitarity for different r_0. See caption of Table II for details.

(N_1,N_2)	r_0/L	$E/E_{\rm box}$	$E/E_{\rm box}$	$\lvert\mathbf{K}\rvert/\left(\frac{2\pi}{L}\right)$
		$N_b\to\infty$	largest N_b	
(2,2)	0.12	0.7182	0.7196	0
	0.1	0.6735	0.6751	
	0.08	0.6232	0.6252	
	0.06	0.5704	0.5730	
	0.04	0.5178	0.5200	
	0.02	0.4675	0.4712	
	0	0.4116(42)	0.4158	
(3,1)	0.12	1.3944	1.3968	0
	0.1	1.4186	1.4218	
	0.08	1.4410	1.4431	
	0.06	1.4604	1.4638	
	0.04	1.4766	1.4826	
	0.02	1.4904	1.5032	
	0	1.5014(187)	1.5201	

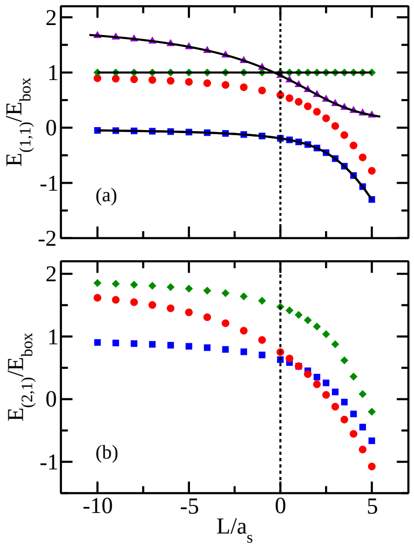

FIG. 3: (Color online) Zero-range energies of (a) the four lowest states of the $(1,1)$ system and (b) the three lowest states of the $(2,1)$ system as a function of L/a_s. The symbols show the lowest ECG energies extrapolated to the $r_0 \to 0$ limit. The solid lines in panel (a) for the $\mathbf{K} = 0$ states are obtained from Lüscher's formula [31, 32].

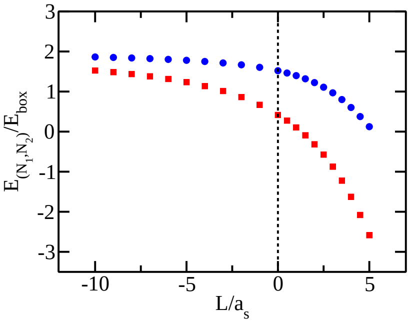

FIG. 4: (Color online) Zero-range energies of the lowest state of the $(2,2)$ and $(3,1)$ systems as a function of L/a_s. Squares and circles show the lowest ECG energy extrapolated to the $r_0 \to 0$ limit for the $(2,2)$ and $(3,1)$ systems, respectively.

levels of the $(1,1)$ and $(2,1)$ systems with zero-range interactions as a function of L/a_s, i.e., throughout the BCS to BEC crossover. The energies are obtained by extrapolating our finite-range ECG energies to the zero-range limit for each a_s/L. In the weakly-attractive BCS regime ($a_s < 0$ and $|a_s|/L \ll 1$), our extrapolated zero-range energies agree with the perturbative energies discussed in Sec. II B. Our $(1,1)$ energies for states with vanishing momentum [squares and triangles in Fig. 3(a)] are in excellent agreement with the energies obtained from Lüscher's formula [see solid lines in Fig. 3(a)] [31, 32]. In the BEC regime ($a_s > 0$ and $a_s/L \ll 1$), the energy spectrum contains two types of energy levels, those where the corresponding states "contain" dimers [e.g., the lowest level in Figs. 3(a) and 3(b)] and those where the corresponding states are best thought of as describing an atomic gas [see triangles and diamonds in Fig. 3(a)]. The dimers consist of fermions that have opposite spin projections. In the $(1,1)$ system, states with vanishing and finite momentum can form s-wave dominated dimers. This can be readily understood by realizing that the total momentum and the orbital angular momentum are distinctly different quantities and that states with finite total momentum contain s-wave contributions [31, 32]. The $(2,1)$ energy spectrum shows a crossing of the two lowest states at $L/a_s \approx 1$. The state with $\hbar|\mathbf{K}| = 2\pi\hbar/L$ has a lower energy in the BCS regime while the state with $\hbar|\mathbf{K}| = 0$ has a lower energy in the BEC regime. This crossing is somewhat similar to the crossing between states with finite and vanishing orbital angular momentum in the harmonically trapped $(2,1)$ system [18, 35, 36].

Squares and circles in Fig. 4 show the extrapolated zero-range energies of the ground state of the $(2,2)$ system and the $(3,1)$ system, respectively, as a function of L/a_s. In the $a_s \to 0^-$ limit, the energies of the $(2,2)$ and $(3,1)$ systems agree. In the $a_s \to 0^+$ limit, in contrast, the energy of the $(2,2)$ system is significantly lower than that of the $(3,1)$ system, reflecting the fact that the $(2,2)$ and $(3,1)$ systems form two dimers and one dimer, respectively.

IV. CONCLUSION

This paper considered the energetics of small two-component Fermi gases in a cubic box with periodic boundary conditions. We treated systems with up to

$N = 4$ atoms using first-order perturbation theory and the explicitly correlated Gaussian basis set expansion approach. We determined the low-lying states throughout the BCS-BEC crossover and carefully analyzed the dependence of the energies on the range of the underlying two-body potential at unitarity. Our calculations agree with results reported in the literature and are expected to serve as benchmarks in the cases where no other literature values exist. The method introduced in this paper extends the application of explicitly correlated Gaussian basis sets, optimized using the stochastic variational method, to quantum few-body problems with periodic boundary conditions.

V. ACKNOWLEDGEMENT

Discussions with D. Kaplan, D. Lee and K. Varga, which motivated this work, correspondence with O. Juillet as well as support by the National Science Foundation (NSF) through Grant No. PHY-1205443 are greatfully acknowledged. This work used the Extreme Science and Engineering Discovery Environment (XSEDE), which is supported by NSF grant number OCI-1053575, and the WSU HPC. This work was additionally supported by the NSF through a grant for the Institute for Theoretical Atomic, Molecular and Optical Physics at Harvard University and Smithsonian Astrophysical Observatory.

Appendix A: Explicitly correlated Gaussian basis functions for systems with periodic boundary conditions

This appendix introduces explicitly correlated Gaussian basis functions that obey periodic boundary conditions and derives analytic expressions for the overlap, kinetic energy and interaction matrix elements. Throughout this appendix, we do not impose symmetry constraints. The proper symmetry of the basis functions can be enforced following Sec. 2.3 of Ref. [22].

The system Hamiltonian H is the sum of the kinetic energy H_0, Eq. (2), and the particle-particle interactions V_{int}, Eq. (3). As discussed in Sec. II C, we imagine that the full three-dimensional space is divided into an infinite number of cubic boxes of length L. The lower left corner of the center box, labeled by $\mathbf{0}$, is located at the origin. Unlike particles are interacting through the finite-range two-body Gaussian potential V_{g}, Eq. (5). To account for the periodicity of the system, we write

$$V_{\text{int}}^{\text{pbc}} = \sum_{a=1}^{N_1} \sum_{b=N_1+1}^{N} \sum_{\mathbf{q}} V_{\text{g}}(\mathbf{x}_{ab} - L\mathbf{q}), \tag{A1}$$

where $\mathbf{q}^T = (q^{(1)}, q^{(2)}, q^{(3)})$ denotes a three-component vector with $q^{(i)} = \cdots, -2, -1, 0, 1, 2, \cdots$. The sum over $\mathbf{q}$ in Eq. (A1) ensures that we are not only considering interactions between pairs of particles of opposite spin in box $\mathbf{0}$ but also interactions of particles in box $\mathbf{0}$ with particles of opposite spin located in other boxes. A key advantage of the Gaussian potential V_{g} is that it factorizes,

$$V_{\text{int}}^{\text{pbc}} = \sum_{a=1}^{N_1} \sum_{b=N_1+1}^{N} U_0 \prod_{i=1}^{3} V_{\text{g}}^{\text{pbc},(i)}(x_{ab}^{(i)} - Lq^{(i)}), \tag{A2}$$

where $V_{\text{g}}^{\text{pbc},(i)}(x_{ab}^{(i)}) = \sum_{\mathbf{q}} \exp[-(x_{ab}^{(i)})^2/(2r_0^2)]$.

1. Basis functions

We first focus on the ith spatial dimension. To construct basis functions $\Psi^{(i)}$ for the ith spatial dimension, we introduce a "single particle" $N \times N$ matrix $B^{(i)}$, a "two-body" $N \times N$ matrix $A^{(i)}$ and a displacement vector $\mathbf{s}^{(i)}$, $\mathbf{s}^{(i)} = (s_1^{(i)}, \cdots, s_N^{(i)})$, and consider the unsymmetrized and non-periodic function $\Psi_{\text{np}}^{(i)}$,

$$\Psi_{\text{np}}^{(i)}(A^{(i)}, B^{(i)}, \mathbf{s}^{(i)}, \mathbf{x}^{(i)}) = \exp\left[-\frac{1}{2}(\mathbf{x}^{(i)})^T A^{(i)} \mathbf{x}^{(i)} - \frac{1}{2}(\mathbf{x}^{(i)} - \mathbf{s}^{(i)})^T B^{(i)} (\mathbf{x}^{(i)} - \mathbf{s}^{(i)})\right], \tag{A3}$$

where $(\mathbf{x}^{(i)})^T = (x_1^{(i)}, \cdots, x_N^{(i)})$. The function $\Psi_{\rm np}^{(i)}$ can alternatively be written in terms of "single particle" Gaussian widths $d_a^{(i)}$ and "two-body" Gaussian widths $d_{ab}^{(i)}$,

$$\Psi_{\rm np}^{(i)}(d_{12}, \cdots, d_{N-1,N}, d_1, \cdots, d_N, \mathbf{s}^{(i)}, \mathbf{x}^{(i)}) = \exp\left[-\sum_{a=1}^{N}\sum_{b=a+1}^{N} \frac{(x_a^{(i)} - x_b^{(i)})^2}{2(d_{ab}^{(i)})^2}\right] \exp\left[-\sum_{a=1}^{N} \frac{(x_a^{(i)} - s_a^{(i)})^2}{2(d_a^{(i)})^2}\right]. \tag{A4}$$

The diagonal elements of the matrix $B^{(i)}$ are related to the $d_a^{(i)}$ by $B_{aa}^{(i)} = 1/(d_a^{(i)})^2$. The off-diagonal elements of $B^{(i)}$ are zero. $A^{(i)}$ is a symmetric matrix constructed from the $N(N-1)/2$ independent Gaussian widths $d_{ab}^{(i)}$. Transforming from relative distance coordinates to single-particle coordinates, we have $A_{ab}^{(i)} = -(d_{ab}^{(i)})^{-2}$ for $a \neq b$ and $A_{aa}^{(i)} = \sum_{b=1, b\neq a}^{N} (d_{ab}^{(i)})^{-2}$.

The function $\Psi_{\rm np}^{(i)}$ introduced in Eq. (A3) does not obey periodic boundary conditions. To enforce periodic boundary conditions, we introduce a sum over the vector $\mathbf{b}^{(i)}$,

$$\Psi^{(i)}(A^{(i)}, B^{(i)}, \mathbf{s}^{(i)}, \mathbf{x}^{(i)}) = \sum_{\mathbf{b}^{(i)}} \Psi_{\rm np}^{(i)}(A^{(i)}, B^{(i)}, \mathbf{s}^{(i)}, \mathbf{x}^{(i)} - L\mathbf{b}^{(i)}), \tag{A5}$$

where $(\mathbf{b}^{(i)})^T = (b_1, b_2, \cdots, b_N)$ with $b_j^{(i)} = \cdots, -2, -1, 0, 1, 2, \cdots$. It can be readily checked that $\Psi^{(i)}(A^{(i)}, B^{(i)}, \mathbf{s}^{(i)}, \mathbf{x}^{(i)} - \mathbf{t})$, where $\mathbf{t}$ is a N-component vector with a single non-zero element, $\mathbf{t}^T = (0, \cdots, 0, L, 0, \cdots, 0)$, equals $\Psi^{(i)}(A^{(i)}, B^{(i)}, \mathbf{s}^{(i)}, \mathbf{x}^{(i)})$, that is, $\Psi^{(i)}$ obeys periodic boundary conditions. The three-dimensional unsymmetrized basis function $\Psi_{\rm 3D}$ is simply the product of the basis functions in the x-, y- and z-directions, i.e., $\Psi_{\rm 3D} = \prod_{i=1}^{3} \Psi^{(i)}$.

2. Overlap matrix element

The overlap between the basis functions $\Psi_{\rm 3D}$ and $\Psi'_{\rm 3D}$ is

$$\langle \Psi_{\rm 3D} | \Psi'_{\rm 3D} \rangle = \prod_{i=1}^{3} \langle \Psi^{(i)} | \Psi'^{(i)} \rangle = \prod_{i=1}^{3} \left[\int_0^L \cdots \int_0^L \Psi^{(i)}(A^{(i)}, B^{(i)}, \mathbf{s}^{(i)}, \mathbf{x}^{(i)}) \Psi^{(i)}(A'^{(i)}, B'^{(i)}, \mathbf{s}'^{(i)}, \mathbf{x}^{(i)}) d\mathbf{x}^{(i)} \right]. \tag{A6}$$

In the following, we focus on the overlap matrix element for the ith dimension. To perform the integration analytically, we shall change the integration limits from $[0, L]$ to $[-\infty, \infty]$. As a first step, we shift the spatial coordinates by defining $\mathbf{x}_{\rm new}^{(i)} = \mathbf{x}^{(i)} - L\mathbf{b}'^{(i)}$ and then renaming $\mathbf{x}_{\rm new}^{(i)}$ as $\mathbf{x}^{(i)}$ for convenience,

$$\begin{aligned} \langle \Psi^{(i)} | \Psi'^{(i)} \rangle &= \sum_{\mathbf{b}^{(i)}} \sum_{\mathbf{b}'^{(i)}} \int_{-Lb_1'^{(i)}}^{L-Lb_1'^{(i)}} \cdots \int_{-Lb_N'^{(i)}}^{L-Lb_N'^{(i)}} \exp\Bigg[-\frac{1}{2}(\mathbf{x}^{(i)} + L\mathbf{b}'^{(i)} - L\mathbf{b}^{(i)})^T A^{(i)} (\mathbf{x}^{(i)} + L\mathbf{b}'^{(i)} - L\mathbf{b}^{(i)}) \\ &\quad -\frac{1}{2}(\mathbf{x}^{(i)} - \mathbf{s}^{(i)} + L\mathbf{b}'^{(i)} - L\mathbf{b}^{(i)})^T B^{(i)} (\mathbf{x}^{(i)} - \mathbf{s}^{(i)} + L\mathbf{b}'^{(i)} - L\mathbf{b}^{(i)}) \Bigg] \times \\ &\quad \exp\left[-\frac{1}{2}(\mathbf{x}^{(i)})^T A'^{(i)} (\mathbf{x}^{(i)}) - \frac{1}{2}(\mathbf{x}^{(i)} - \mathbf{s}'^{(i)})^T B'^{(i)} (\mathbf{x}^{(i)} - \mathbf{s}'^{(i)}) \right] d\mathbf{x}^{(i)}. \end{aligned} \tag{A7}$$

Next, we replace $\mathbf{b}^{(i)} - \mathbf{b}'^{(i)}$ by $\Delta\mathbf{b}^{(i)}$ and replace the sum over $\mathbf{b}^{(i)}$ by a sum over $\Delta\mathbf{b}^{(i)}$,

$$\begin{aligned} \langle \Psi^{(i)} | \Psi'^{(i)} \rangle &= \sum_{\Delta\mathbf{b}^{(i)}} \sum_{\mathbf{b}'^{(i)}} \int_{-Lb_1'^{(i)}}^{L-Lb_1'^{(i)}} \cdots \int_{-Lb_N'^{(i)}}^{L-Lb_N'^{(i)}} \exp\Bigg[-\frac{1}{2}(\mathbf{x}^{(i)} - L\Delta\mathbf{b}^{(i)})^T A^{(i)} (\mathbf{x}^{(i)} - L\Delta\mathbf{b}^{(i)}) \\ &\quad -\frac{1}{2}(\mathbf{x}^{(i)} - \mathbf{s}^{(i)} - L\Delta\mathbf{b}^{(i)})^T B^{(i)} (\mathbf{x}^{(i)} - \mathbf{s}^{(i)} - L\Delta\mathbf{b}^{(i)}) \Bigg] \times \\ &\quad \exp\left[-\frac{1}{2}(\mathbf{x}^{(i)})^T A'^{(i)} (\mathbf{x}^{(i)}) - \frac{1}{2}(\mathbf{x}^{(i)} - \mathbf{s}'^{(i)})^T B'^{(i)} (\mathbf{x}^{(i)} - \mathbf{s}'^{(i)}) \right] d\mathbf{x}^{(i)}. \end{aligned} \tag{A8}$$

Since the integrand is independent of $\mathbf{b}'^{(i)}$, the sum over $\mathbf{b}'^{(i)}$ changes the integration limits of the N integrals to $[-\infty,\infty]$. Renaming $\Delta\mathbf{b}^{(i)}$ as $\mathbf{b}^{(i)}$ for convenience, we find

$$\begin{aligned}\langle\Psi^{(i)}|\Psi'^{(i)}\rangle \;=\; & \sum_{\mathbf{b}^{(i)}}\int_{-\infty}^{\infty}\cdots\int_{-\infty}^{\infty}\exp\Bigg[-\frac{1}{2}(\mathbf{x}^{(i)}-L\mathbf{b}^{(i)})^T A^{(i)}(\mathbf{x}^{(i)}-L\mathbf{b}^{(i)}) \\ & -\frac{1}{2}(\mathbf{x}^{(i)}-\mathbf{s}^{(i)}-L\mathbf{b}^{(i)})^T B^{(i)}(\mathbf{x}^{(i)}-\mathbf{s}^{(i)}-L\mathbf{b}^{(i)})\Bigg]\times \\ & \exp\left[-\frac{1}{2}(\mathbf{x}^{(i)})^T A'^{(i)}(\mathbf{x}^{(i)})-\frac{1}{2}(\mathbf{x}^{(i)}-\mathbf{s}'^{(i)})^T B'^{(i)}(\mathbf{x}^{(i)}-\mathbf{s}'^{(i)})\right]d\mathbf{x}^{(i)}.\end{aligned} \tag{A9}$$

In going from Eq. (A6) to Eq. (A9), we have transformed the integrals over box $\mathbf{0}$ to integrals over all space.

Pulling $\mathbf{x}^{(i)}$-independent terms out of the integrals, Eq. (A9) becomes

$$\begin{aligned}\langle\Psi^{(i)}|\Psi'^{(i)}\rangle = \sum_{\mathbf{b}^{(i)}}\mathcal{C}^{(i)}(A^{(i)},B^{(i)},\mathbf{s}^{(i)},\mathbf{b}^{(i)})\int_{-\infty}^{\infty}...\int_{-\infty}^{\infty} \quad & g\left(A^{(i)}(L\mathbf{b}^{(i)})+B^{(i)}(L\mathbf{b}^{(i)}+\mathbf{s}^{(i)});A^{(i)}+B^{(i)},\mathbf{x}^{(i)}\right)\times \\ & g\left(B'^{(i)}\mathbf{s}'^{(i)};A'^{(i)}+B'^{(i)},\mathbf{x}^{(i)}\right)d\mathbf{x}^{(i)},\end{aligned} \tag{A10}$$

where

$$\begin{aligned}& \mathcal{C}^{(i)}(A^{(i)},B^{(i)},\mathbf{s}^{(i)},\mathbf{b}^{(i)}) = \\ & \exp\left[-\frac{1}{2}(L\mathbf{b}^{(i)})^T A^{(i)}(L\mathbf{b}^{(i)})-\frac{1}{2}(L\mathbf{b}^{(i)}+\mathbf{s}^{(i)})^T B^{(i)}(L\mathbf{b}^{(i)}+\mathbf{s}^{(i)})-\frac{1}{2}(\mathbf{s}'^{(i)})^T B'^{(i)}\mathbf{s}'^{(i)}\right]\end{aligned} \tag{A11}$$

and

$$g(\mathbf{h};D,\mathbf{x}) = \exp\left(-\frac{1}{2}\mathbf{x}^T D\mathbf{x}+\mathbf{h}^T\mathbf{x}\right) \tag{A12}$$

is the generating function defined in Eq. (6.19) of Ref. [22]. Using Eqs. (7.22) and (7.23) of Ref. [22], we find

$$\int_{-\infty}^{\infty}...\int_{-\infty}^{\infty}g(\mathbf{h};D,\mathbf{x})g(\mathbf{h}';D',\mathbf{x})d\mathbf{x} = \left(\frac{(2\pi)^N}{\det C}\right)^{1/2}\exp\left(\frac{1}{2}\mathbf{v}^T C^{-1}\mathbf{v}\right) \tag{A13}$$

with $C = D+D'$ and $\mathbf{v} = \mathbf{h}+\mathbf{h}'$. Substituting $D = A^{(i)}+B^{(i)}$, $D' = A'^{(i)}+B'^{(i)}$, $\mathbf{h} = A^{(i)}(L\mathbf{b}^{(i)})+B^{(i)}(L\mathbf{b}^{(i)}+\mathbf{s}^{(i)})$ and $\mathbf{h}' = B'^{(i)}\mathbf{s}'^{(i)}$, we find

$$\langle\Psi^{(i)}|\Psi'^{(i)}\rangle = \sum_{\mathbf{b}^{(i)}}\mathcal{C}^{(i)}(A^{(i)},B^{(i)},\mathbf{s}^{(i)},\mathbf{b}^{(i)})\left(\frac{(2\pi)^N}{\det\left(C^{(i)}\right)}\right)^{1/2}\exp\left[\frac{1}{2}(\mathbf{v}^{(i)})^T(C^{(i)})^{-1}\mathbf{v}^{(i)}\right], \tag{A14}$$

where

$$C^{(i)} = A^{(i)}+B^{(i)}+A'^{(i)}+B'^{(i)} \tag{A15}$$

and

$$\mathbf{v}^{(i)} = A^{(i)}(L\mathbf{b}^{(i)})+B^{(i)}(L\mathbf{b}^{(i)}+\mathbf{s}^{(i)})+B'^{(i)}\mathbf{s}'^{(i)}. \tag{A16}$$

3. Kinetic energy matrix element

The kinetic energy matrix element is given by

$$\langle\Psi_{3\mathrm{D}}|H_0|\Psi'_{3\mathrm{D}}\rangle = \sum_{i=1}^{3}\left[\langle\Psi^{(i)}|H_0^{(i)}|\Psi'^{(i)}\rangle\left(\prod_{j=1,j\neq i}^{3}\langle\Psi^{(j)}|\Psi'^{(j)}\rangle\right)\right], \tag{A17}$$

where $\langle\Psi^{(i)}|\Psi'^{(i)}\rangle$ is given in Eq. (A14) and where $H_0^{(i)} = \sum_{a=1}^{N} \frac{-\hbar^2}{2m}\frac{\partial^2}{\partial(x_a^{(i)})^2}$. Thus we only need to evaluate the kinetic energy matrix element for the ith dimension. Following steps similar to those detailed in Sec. A 2, we find

$$\langle\Psi^{(i)}|H_0^{(i)}|\Psi'^{(i)}\rangle = \sum_{\mathbf{b}^{(i)}} \frac{\hbar^2}{2}\left[\mathrm{Tr}\left((A^{(i)}+B^{(i)})(C^{(i)})^{-1}(A'^{(i)}+B'^{(i)})\Lambda\right) - (\mathbf{y}^{(i)})^T\Lambda\mathbf{y}^{(i)}\right]\langle\Psi^{(i)}|\Psi'^{(i)}\rangle, \tag{A18}$$

where

$$\mathbf{y}^{(i)} = (A'^{(i)}+B'^{(i)})(C^{(i)})^{-1}\left[B^{(i)}(L\mathbf{b}^{(i)}+\mathbf{s}^{(i)}) + A^{(i)}(L\mathbf{b}^{(i)})\right] - (A^{(i)}+B^{(i)})(C^{(i)})^{-1}(B'^{(i)}\mathbf{s}'^{(i)}) \tag{A19}$$

and Λ is a $N\times N$ diagonal matrix with diagonal elements $\Lambda_{jj} = 1/m_j$; here, m_j is the mass of the jth atom (in our case, $m_j = m$).

4. Interaction matrix element

The result for the interaction matrix element $\langle\Psi_{3\mathrm{D}}|V_{\mathrm{int}}^{\mathrm{pbc}}|\Psi'_{3\mathrm{D}}\rangle$ can be readily constructed from the matrix elements $\langle\Psi^{(i)}|V_{\mathrm{g}}^{\mathrm{pbc},(i)}|\Psi'^{(i)}\rangle$. To evaluate $\langle\Psi^{(i)}|V_{\mathrm{g}}^{\mathrm{pbc},(i)}|\Psi'^{(i)}\rangle$, we define $\mathbf{x}_{\mathrm{new}}^{(i)} = \mathbf{x}^{(i)} - L\mathbf{b}'^{(i)}$ and then rename $\mathbf{x}_{\mathrm{new}}^{(i)}$ as $\mathbf{x}^{(i)}$ for convenience,

$$\begin{aligned}\langle\Psi^{(i)}|V_{\mathrm{g}}^{\mathrm{pbc},(i)}|\Psi'^{(i)}\rangle = {} & \sum_{\Delta\mathbf{b}^{(i)}}\sum_{\mathbf{b}'^{(i)}}\int_{-Lb_1'^{(i)}}^{L-Lb_1'^{(i)}}\cdots\int_{-Lb_N'^{(i)}}^{L-Lb_N'^{(i)}} \exp\Big[-\frac{1}{2}(\mathbf{x}^{(i)}-L\Delta\mathbf{b}^{(i)})^T A^{(i)}(\mathbf{x}^{(i)}-L\Delta\mathbf{b}^{(i)}) \\ & -\frac{1}{2}(\mathbf{x}^{(i)}-\mathbf{s}^{(i)}-L\Delta\mathbf{b}^{(i)})^T B^{(i)}(\mathbf{x}^{(i)}-\mathbf{s}^{(i)}-L\Delta\mathbf{b}^{(i)})\Big] \\ & \left[\sum_{q^{(i)}}\exp\left(-\frac{(x_a^{(i)}-x_b^{(i)}+L{b'_a}^{(i)}-L{b'_b}^{(i)}-Lq^{(i)})^2}{2r_0^2}\right)\right] \\ & \exp\left[-\frac{1}{2}(\mathbf{x}^{(i)})^T A'^{(i)}(\mathbf{x}^{(i)}) - \frac{1}{2}(\mathbf{x}^{(i)}-\mathbf{s}'^{(i)})^T B'^{(i)}(\mathbf{x}^{(i)}-\mathbf{s}'^{(i)})\right] d\mathbf{x}^{(i)}.\end{aligned} \tag{A20}$$

Next, we replace $q^{(i)} - {b'_a}^{(i)} + {b'_b}^{(i)}$ by $q_{\mathrm{new}}^{(i)}$. Since ${b'_a}^{(i)}$ and ${b'_b}^{(i)}$ are fixed, both $q_{\mathrm{new}}^{(i)}$ and $q^{(i)}$ run through all integers. This implies that we can replace the sum over $q^{(i)}$ by a sum over $q_{\mathrm{new}}^{(i)}$. We then rewrite $q_{\mathrm{new}}^{(i)}$ as $q^{(i)}$ for convenience,

$$\begin{aligned}\langle\Psi^{(i)}|V_{\mathrm{g}}^{\mathrm{pbc},(i)}|\Psi'^{(i)}\rangle = {} & \sum_{\Delta\mathbf{b}^{(i)}}\sum_{\mathbf{b}'^{(i)}}\int_{-Lb_1'^{(i)}}^{L-Lb_1'^{(i)}}\cdots\int_{-Lb_N'^{(i)}}^{L-Lb_N'^{(i)}} \exp\Big[-\frac{1}{2}(\mathbf{x}^{(i)}-L\Delta\mathbf{b}^{(i)})^T A^{(i)}(\mathbf{x}^{(i)}-L\Delta\mathbf{b}^{(i)}) \\ & -\frac{1}{2}(\mathbf{x}^{(i)}-\mathbf{s}^{(i)}-L\Delta\mathbf{b}^{(i)})^T B^{(i)}(\mathbf{x}^{(i)}-\mathbf{s}^{(i)}-L\Delta\mathbf{b}^{(i)})\Big]\left[\sum_{q^{(i)}}\exp\left(-\frac{(x_a^{(i)}-x_b^{(i)}-Lq^{(i)})^2}{2r_0^2}\right)\right] \\ & \exp\left[-\frac{1}{2}(\mathbf{x}^{(i)})^T A'^{(i)}(\mathbf{x}^{(i)}) - \frac{1}{2}(\mathbf{x}^{(i)}-\mathbf{s}'^{(i)})^T B'^{(i)}(\mathbf{x}^{(i)}-\mathbf{s}'^{(i)})\right] d\mathbf{x}^{(i)}.\end{aligned} \tag{A21}$$

Lastly, changing the sum over $\mathbf{b}'^{(i)}$ to an integral and following steps similar to those discussed in Sec. A 2, we find

$$\begin{aligned}& \langle\Psi^{(i)}|V_{\mathrm{g}}^{\mathrm{pbc},(i)}|\Psi'^{(i)}\rangle = \\ & \sum_{\mathbf{b}^{(i)}}\sum_{q^{(i)}}\left(\frac{c^{(i)}}{c^{(i)}+2\rho}\right)^{1/2}\exp\left\{-\frac{c^{(i)}\rho}{c^{(i)}+2\rho}\left[\left((C^{(i)})^{-1}\mathbf{v}^{(i)}\right)_a - \left((C^{(i)})^{-1}\mathbf{v}^{(i)}\right)_b - Lq^{(i)}\right]^2\right\}\langle\Psi^{(i)}|\Psi'^{(i)}\rangle,\end{aligned} \tag{A22}$$

where $(c^{(i)})^{-1} = [(C^{(i)})^{-1}]_{aa} + [(C^{(i)})^{-1}]_{bb} - [(C^{(i)})^{-1}]_{ab} - [(C^{(i)})^{-1}]_{ba}$ and $\rho = 1/(2r_0^2)$.

---

[1] S. Giorgini, L. P. Pitaevskii, and S. Stringari, Rev. Mod. Phys. **80**, 1215 (2008).

[2] I. Bloch, J. Dalibard, and W. Zwerger, Rev. Mod. Phys.

80, 885 (2008).

[3] W. Ketterle and M. W. Zwierlein, *Making, probing and understanding ultracold Fermi gases.* Ultracold Fermi Gases, Proceedings of the International School of Physics "Enrico Fermi", Course CLXIV, Varenna, 20 - 30 June 2006, edited by M. Inguscio, W. Ketterle, and C. Salomon, IOS Press, Amsterdam (2008).

[4] D. Blume. Progress in Physics **75**, 046401 (2012).

[5] A. Gezerlis and J. Carlson, *Terrestrial and Astrophysical Superfluidity: Cold Atoms and Neutron Matter.* arXiv:1109.4946 (to appear as a chapter in "The Neutron Star Crust", edited by C. A. Bertulani and J. Piekarewicz).

[6] C. Chin, R. Grimm, P. Julienne, and E. Tiesinga, Rev. Mod. Phys. **82**, 1225 (2010).

[7] J. Carlson, S.-Y. Chang, V. R. Pandharipande, and K. E. Schmidt, Phys. Rev. Lett. **91**, 050401 (2003).

[8] G. E. Astrakharchik, J. Boronat, J. Casurlleras, and S. Giorgini, Phys. Rev. Lett. **93**, 200404 (2004).

[9] A. Bulgac, J. E. Drut, and P. Magierski, Phys. Rev. Lett. **96**, 090404 (2006).

[10] E. Burovski, N. Prokof'ev, B. Svistunov, and M. Troyer, Phys. Rev. Lett. **96**, 160402 (2006).

[11] O. Juillet, New J. Phys. **9**, 163 (2007).

[12] J. Carlson, S. Gandolfi, K. E. Schmidt, and S. Zhang, Phys. Rev. A **84**, 061602(R) (2011).

[13] M. G. Endres, D. B. Kaplan, J.-W. Lee and A. N. Nicholson, Phys. Rev. A **84**, 043644, (2011).

[14] S. Bour, X. Li, D. Lee, U. Meiβner, and L. Mitas, Phys. Rev. A **83**, 063619 (2011).

[15] H. H. B. Sørensen, D. V. Fedorov, and A. S. Jensen, Nuclei and Mesoscopic Physics, ed. by V. Zelevinsky, AIP Conf. Proc. No. 777 (AIP, Melville, NY, 2005), p. 12.

[16] J. von Stecher and C. H. Greene, Phys. Rev. Lett. **99**, 090402 (2007).

[17] D. Blume, J. von Stecher and C. H. Greene, Phys. Rev. Lett. **99**, 233201 (2007).

[18] J. von Stecher, C. H. Greene, and D. Blume, Phys. Rev. A **77**, 043619 (2008).

[19] K. M. Daily and D. Blume, Phys. Rev. A **81**, 053615 (2010).

[20] D. Blume and K. M. Daily, C. R. Physique **12**, 86 (2011).

[21] D. Rakshit, K. M. Daily, and D. Blume, Phys. Rev. A **85**, 033634 (2012).

[22] Y. Suzuki and K. Varga, *Variational Approach to Quantum Mechanical Few-Body Problems* (Springer Verlag, Berlin, 1998).

[23] J. Mitroy, S. Bubin, W. Horiuchi, Y. Suzuki, L. Adamowicz, W. Cencek, K. Szalewicz, J. Komasa, D. Blume, and K. Varga, accepted for publication in Review of Modern Physics.

[24] L. Pricoupenko and Y. Castin, J. Phys. A **40**, 12863 (2007).

[25] S. R. Beane, E. Chang, W. Deltmold, B. Joo, H. W. Lin, T. C. Luu, K. Orginos, A. Parreno, M. J. Savage, A. Torok, and A. Walker-Loud, Phys. Rev. Lett. **106**, 162001 (2011).

[26] S. R. Beane, W. Detmold, and M. J. Savage, Phys. Rev. D **76**, 074507 (2007).

[27] V. I. Kukulin and V. M. Krasnpol'sky, J. Phys. G **3**, 795 (1977).

[28] E. Fermi, Nuovo Cimento **11**, 157 (1934).

[29] K. Varga reported on the usage of explicitly correlated Gaussian basis functions to periodic molecular hydrogen chains at the workshop entitled "Weakly-Interacting Few-Body Systems", July 4-8, 2011, at the ETC*.

[30] R. G. Newton, *Scattering Theory of Waves and Particles*, Second Edition, Dover Publications, Inc., Mineola, New York, 2002.

[31] M. Lüscher, Commun. Math. Phys. **105**, 153 (1986).

[32] M. Lüscher, Nucl. Phys. **B354**, 531 (1991).

[33] F. Werner and Y. Castin, Phys. Rev. A **86**, 013626 (2012); see Fig. 1(a).

[34] The $(2,1)$ state with finite momentum has been considered by O. Juillet using lattice Monte Carlo techniques, private communication (2013).

[35] J. P. Kestner and L.-M. Duan, Phys. Rev. A **76**, 033611 (2007).

[36] I. Stetcu, B. R. Barrett, U. van Kolck, and J. P. Vary, Phys. Rev. A **76**, 063613 (2007).